Journal of Power Sources 475 (2020) 228633

Contents lists available at ScienceDirect

Journal of Power Sources

journal homepage: www.elsevier.com/locate/jpowsour

High performance flow through microbial fuel cells with anion exchange membrane

Ruggero Rossi [a], Xu Wang [b], Bruce E. Logan [a,*]

[a] Department of Civil and Environmental Engineering, The Pennsylvania State University, University Park, PA, 16802, USA
[b] School of Resource and Environmental Sciences, Hubei International Scientific and Technological Cooperation Base of Sustainable Resource and Energy, Wuhan University, 129 Luoyu Road, Wuhan, 430079, PR China

HIGHLIGHTS

- An AEM was used in a MEA MFC to enhance hydroxide ions transport between electrodes.
- Maximum power density of 5.7 ± 0.4 W m^{-2} was obtained in 50 mM PBS.
- Maximum power density increased to 7.1 ± 0.4 W m^{-2} in 100 mM PBS.
- MFC assembled internal resistance was lower than individual electrode resistances.

ARTICLE INFO

Keywords:
MFC
Flow cell
MEA
AEM
Power density

ABSTRACT

Microbial fuel cells (MFCs) can be limited to low power densities due to impacts of localized pH on electrode performance. Acidification of the anodic biofilm limits current generation by bacteria and the increase in cathode pH due to the oxygen reduction reaction reduces the whole cell potential. In this study, an anion exchange membrane (AEM) was used to make a membrane electrode assembly (MEA) in an MFC, with the anode, AEM, and cathode close together to enhance hydroxide ions transport from cathode to anode to minimize pH imbalances and reduce electrode spacing. With a flow-through felt anode the MFC produced 5.7 ± 0.4 W m^{-2} (at 29 ± 1 A m^{-2}, internal resistance of 7.2 ± 0.6 mΩ m^2, based on cross sectional area), which is one of the highest power densities produced in an MFC using a 50 mM phosphate buffer (PBS). Reducing the flowrate of the anolyte or air past the cathode decreased performance. Increasing the buffer concentration to 100 mM produced a maximum power density of 7.1 ± 0.4 W m^{-2}, the highest power density ever recorded for an MFC, demonstrating the importance of buffer concentration in maintaining favorable localized pHs.

1. Introduction

Increasing maximum power densities of microbial fuel cells (MFCs) is one of the greatest challenges for the application of this technology in renewable energy production [1–3]. Maximum power densities of MFCs can be limited by the development of pH imbalances between the anode and the cathode due to electrochemical reactions [4–6]. The anodic oxidation of 1 mole of acetate generates 8 moles of protons and 8 moles of electrons while the oxygen reduction reaction (ORR) at the cathode produces just as many hydroxide ions. If the solution in contact with the electrode is not well buffered, the pH at the anode will decrease, inhibiting or damaging the microbial biofilm and thus reducing the maximum current densities produced by the MFC [7]. At the cathode, the accumulation of hydroxide ions will increase the solution pH and reduce the cathode potential by 59 mV per unit of pH, based on the Nernst equation [8]. Thus, new approaches need to be identified to improve the overall MFC performance and overcome the limitations due to pH imbalance between the electrodes.

Using high buffer concentrations help in maintaining a stable pH near the electrode surfaces [4,6,9]. Most studies reporting large maximum power densities have used buffer concentrations up to 200 mM, with improvements demonstrated through comparisons to less concentrated buffers that could not be explained only by the lower solution resistances [9]. For example, a maximum power density of 4.7 ± 0.2 W m^{-2} obtained using 200 mM phosphate buffer (PBS) was more than 80% larger than that obtained in 50 mM PBS (2.6 ± 0.05 W m^{-2}) in

* Corresponding author.
E-mail address: blogan@psu.edu (B.E. Logan).

https://doi.org/10.1016/j.jpowsour.2020.228633
Received 25 April 2020; Received in revised form 17 June 2020; Accepted 8 July 2020
Available online 7 August 2020

an MFC with the same configuration [10]. However, the anodic biofilm is adversely impacted by buffer concentrations larger than 200 mM, due to the high concentration of salts in the media [9]. In another study a maximum power density of 5.9 ± 0.5 W m^{-2} was obtained in a 70 mM carbonate/phosphate buffer amended with potassium chloride to increase the solution conductivity and minimize solution resistance [2]. While the highest power density of 6.8 W m^{-2} was previously achieved in 200 mM PBS, it required a cathode much larger (14×) than the anode, and thus the power output normalized to the cathode or the cross sectional area as done in other studies was much lower [11,12].

Reducing the electrode spacing can also increase the MFC performance mainly by decreasing the solution resistance, even though few studies reported an improved transport of protons due to the smaller spacing [4,13,14]. When the distance between anode and cathode is reduced, a separator needs to be inserted between the electrodes to avoid short circuiting [15,16]. Several separators have been examined in MFCs [17]. For example, a cloth electrode assembly (CEA) configuration, with anode and cathode separated by a thin fabric, produced 3.70 W m^{-2} (13 A m^{-2}) in 50 mM PBS [14]. In that study, the maximum current density doubled to 20 A m^{-2} by reducing the thickness of the separator by half, from 0.6 mm to 0.3 mm, which was claimed to increase the power by enhancing proton transport between the electrodes [14]. However, it was not demonstrated that protons transport was actually enhanced by using that separator. It was shown by others that cation species (other than protons) in the MFC with a cation exchange membrane (CEM) were mainly used to balance electron transfer due to their higher concentrations, resulting in the development of pH imbalances in the two chambers [18,19]. Hydroxide ion transport away from the cathode is likely to be more important for MFC performance than proton transport from the anode to the cathode. At neutral to alkaline pH the ORR occurs through the release of hydroxide ions (eq. (1)) rather than consumption of protons that occurs under acidic pH [8], according to:

$$O_2 + 4e^- + 2H_2O \rightleftharpoons 4OH^- \quad E_{Cat} = +815mV \tag{1}$$

Thus, anion exchange membranes (AEMs) are a better choice for MFCs than CEMs.

Reducing the electrode spacing can improve the MFC performance by decreasing the internal resistance, but a close electrode spacing can increase the oxygen intrusion to the anode [20–24] and reduce power production. For example, in a study reporting the highest maximum power density with equally sized electrodes (5.9 ± 0.5 W m^{-2}) in a carbonate/phosphate buffer at 40 °C and 4 mm electrode spacing, there was a large decrease in performance after only two days of operation, likely due to oxygen intrusion, to 4.8 ± 0.1 W m^{-2}, and the initial maximum power density was never recovered, even after replacing the cathode [2].

In this study, we investigated the performance of a flow cell MFC in a membrane electrode assembly (MEA) configuration. In contrast to other MFC studies using an MEA configuration, an AEM rather than a CEM was used to facilitate hydroxide ion transport. The carbon felt anode and an air cathode (no catholyte) were pressed onto the AEM, ensuring a small electrode spacing but facilitating transport of only hydroxide ions produced at the cathode by the ORR through the membrane (Fig. 1). Cation transport is severely limited through the AEM while hydroxide anion transport is enhanced due to development of a localized concentration gradient and enhanced ion transport to the anode due to the electric field (i.e. from cathode to anode) when the current density is sufficiently high. Oxygen intrusion was controlled by pumping air in the cathode chamber at different flowrates. To further minimize internal resistance the flow was directed through the felt anode, and its flowrate was also controlled to improve overall MFC performance. While previous research has investigated the use of small electrode spacing with cloth or CEM separators in MFCs [14,25], this is the first study focusing on AEM-MFCs and hydroxide ion transport.

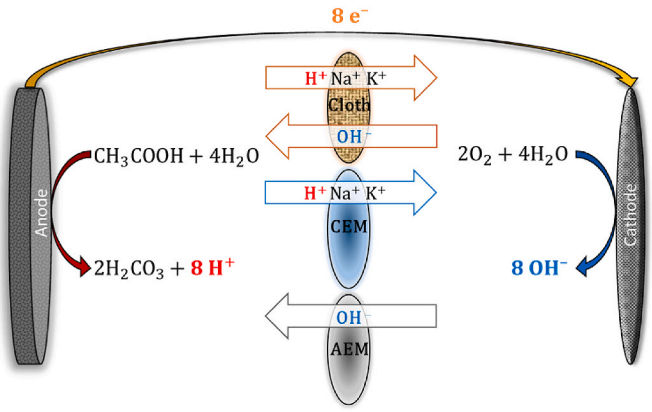

Fig. 1. Comparison of the ion transport in MFCs with cloth separator, cation exchange membrane (CEM) or anion exchange membrane (AEM). Note that the cathode reaction is balanced by release of hydroxide ions and not consumption of protons. Only the AEM can selectively enhance hydroxide ion transport from the cathode and thus control charge balance through hydroxide ion transport rather than proton ion transport.

2. Materials and methods

2.1. Construction and operation of the MFCs

The MFCs were made with two-chambers, with the anolyte flowing through the anode chamber and only air flowing through the air-cathode chamber. There was no catholyte as the MEA cathode was pressed against the anode. By using a cathode chamber, it was possible to control the air flow past the cathode and avoid excessive oxygen intrusion (Fig. 2). The two cylindrical chambers (30 mm exposed diameter, 7 cm^2 effective area), each containing one of the electrodes, were separated by an AEM (106 ± 1 μm thick with an ion exchange capacity of 1.85 mmol g^{-1}, Selemion AMV-N, Asahi Glass, Co., Tokyo, Japan). The anolyte flowed from the top to the bottom of the anode chamber while the air followed the same direction through the cathode chamber. The anode chamber was made of a compressible silicon gasket with its volume completely occupied by the carbon felt in order to force the anolyte flow through the anode and avoid the development of preferential flow paths within the chamber. A carbon felt of the same dimension of the anode chamber (7 cm^2 area, 6.35 mm thick, Alfa Aesar) was positioned against the AEM. Three layers of plastic mesh spacers (S1.5, 30PTFE-625P, Dexmet Corp.) were used in the cathode chamber to press the cathode against the AEM to achieve an effective MEA configuration and to enable air flow in the cathode chamber through their large porosity. Titanium foils were used as current collectors in both anode and cathode chambers.

The carbon felt anode was heat treated at 450 °C in a furnace for 30 min prior to use [24,26]. An anion-exchange cathode catalyst ink was prepared by blending carbon-supported catalysts (10% Pt/C) with quaternary 1,4-diazabicyclo-[2.2.2]-octane (DABCO) polysulphone (QDPSU) solution in dimethylacetamide (DMAc) [27,28]. The ink was sonicated for 1 h and then sprayed onto one side of a four-layer PTFE diffusion layer (DL), wet-proofed carbon clot for a final a Pt loading of 0.5 mg cm^{-2}. Cathode and AEM were cold-pressed at 1000 kg cm^{-2} for 10 min resulting in the final MEA used in the MFC.

The anolyte (500 mL) was recirculated through the carbon felt at a flow rate of 5 mL min^{-1} except as noted. Based on an empty volume of the anode chamber of 4.4 mL, the correspondent empty bed hydraulic retention time (HRT) at 5 mL min^{-1} was 53 s. The 50 mM phosphate buffer solution (PBS; 4.58 g L^{-1} Na_2HPO_4, 2.45 g L^{-1} NaH_2PO_4 H_2O, 0.31 g L^{-1} NH_4Cl, 0.13 g L^{-1} KCl, conductivity of 6.93 mS cm^{-1}) used as the anolyte had a pH = 7.0 ± 0.1, and it was amended with 12.5 mL L^{-1} of a concentrated trace mineral solution, 5 mL L^{-1} of a vitamin solution,

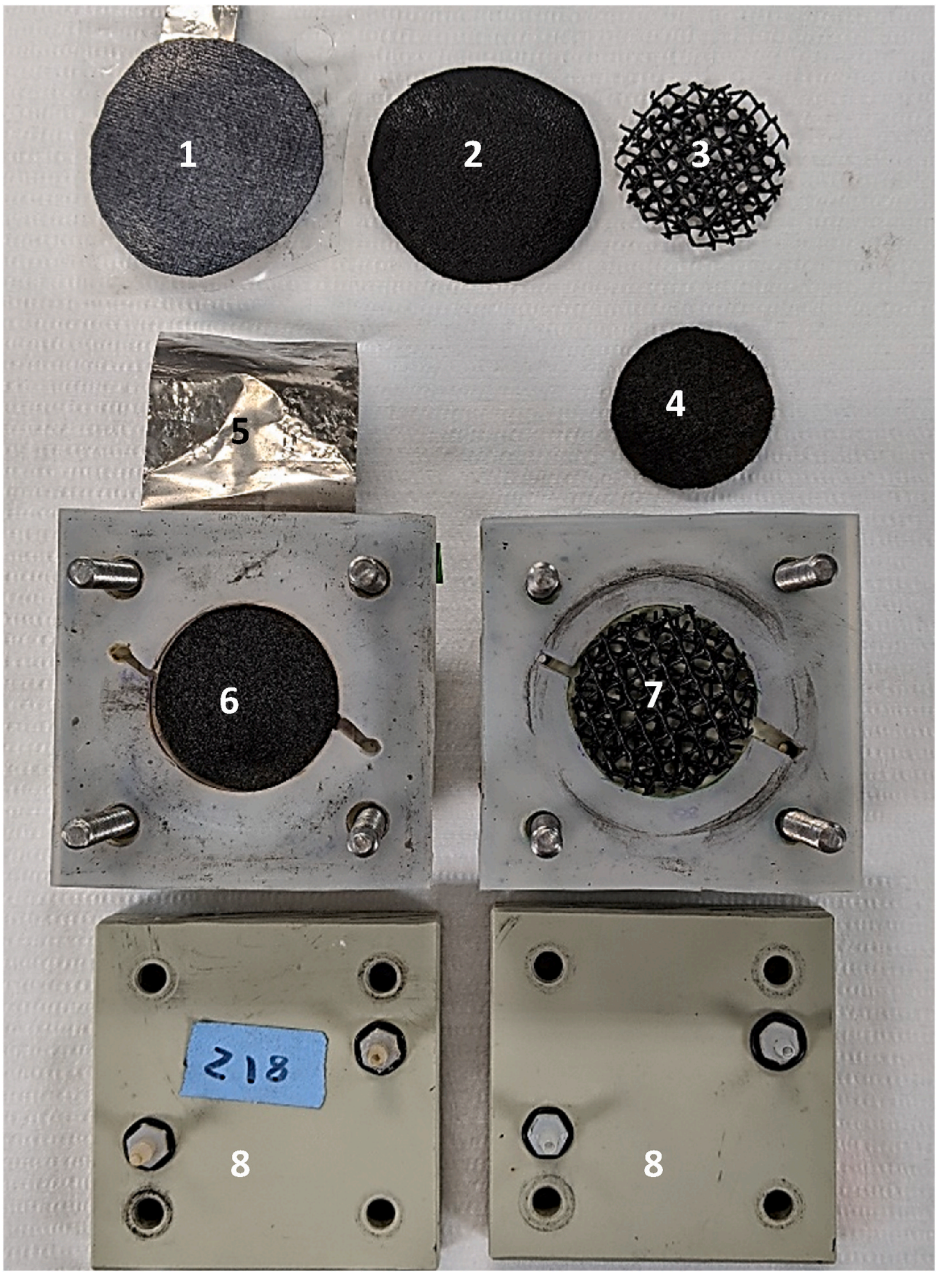

Fig. 2. Photographs of the MFC materials used in this study. (1) Cathode MEA, air-side; (2) cathode, solution side; (3) spacers; (4) carbon felt anode; (5) anode current collector; (6) anode chamber; (7) cathode chamber; and (8) end-plates.

and sodium acetate (2 g L^{-1}) [29]. In one test, a 100 mM PBS anolyte was used (PBS_{100}; 9.15 g L^{-1} Na_2HPO_4, 4.90 g L^{-1} NaH_2PO_4 H_2O, 0.62 g L^{-1} NH_4Cl, 0.26 g L^{-1} KCl, conductivity of 11.93 mS cm^{-1}). The air was pumped in the cathode chamber at a flow rate of 2 mL min^{-1} (empty bed HRT of 133 s), except otherwise noted, and was first humidified by directing the flow through deionized water in a half full glass bottle (1000 mL). The MFCs were operated in duplicate with a fixed external resistance of 20 Ω in a temperature-controlled room at 30 °C.

2.2. Electrochemical measurements

The carbon felt anode was acclimated at a constant potential of +200 mV vs SHE to maximize the microbial energy harvest and minimize the impact of the external resistance on the electrode operation [9, 30]. The acclimation was performed in cubic-shaped reactors constructed from polycarbonate blocks with an inside cylindrical chamber 3 cm in diameter and 4 cm in length filled with 50 mM PBS and inoculated with the effluent of MFCs operating for >1 year while used in other experiments. Electrochemical tests on the cathodes were conducted (duplicates) in 4 cm long and 3 cm diameter electrochemical cells with an empty volume of 28 mL with the cathode as the working electrode and a Pt mesh (3 cm^2 projected area) as a counter electrode, placed 3 cm far from the cathode. The reference electrode (RE) used to measure the electrode potentials (Single junction silver chloride (Ag/AgCl) reference electrode; model RREF0021, Pine Research Instrumentation, NC; + 199 mV versus a standard hydrogen electrode, SHE) was placed in the current path between the electrodes, 1 cm distant from the cathode [28]. An AEM (Selemion AMV-N, Asahi Glass, Co., Tokyo, Japan) was placed between the cathode/RE chamber and the Pt counter electrode when electrochemical tests were conducted on the cathode. This configuration allowed evaluation of the cathode performance avoiding the interference of an anodic biofilm as the counter electrode [6].

To investigate the individual electrode performance, linear sweep voltammetries (LSVs) were conducted on the felt anode at the end of the acclimation period and on the cathode and MEA cathode. LSVs were conducted at a scan rate of 0.1 mV s^{-1} from the open circuit potential (OCP) to +200 mV (anode) and −300 mV (cathode). Prior to the LSVs the working electrodes were left for 2 h at the OCP and then a fast EIS (from 100 kHz to 500 Hz, 5 mV amplitude, 10 points s^{-1}, ≈25 s $scan^{-1}$) was recorded at the OCP to calculate the solution resistance (R_Ω) [31]. The reported electrode potentials were corrected based on R_Ω [31,32]. The measured electrode potentials (not corrected for R_Ω) are reported in the Supporting Information. The RE used to measure the electrode potentials was placed in the current path between the electrodes [31,32].

The performance of the electrodes was examined using the electrode potential slope (EPS) method [13]. Following a rapid change in the electrode potentials due to activation losses over an initial limited range of low current densities, the electrode potentials become proportional to the current density. Under these circumstances, for the EPS analysis a linearized portion of the electrode potentials in a current density range typical for maximum power densities in MFCs was used to assess anodic ($E_{An,e0}$) and cathodic ($E_{Cat,e0}$) potentials under the experimental conditions to better describe the electrode performance in terms of experimental electrode potentials. The slopes of the linearized portion of the electrode potentials were used to calculate the anode (R_{An}) and cathode (R_{Cat}) resistances, with the solution resistance (R_Ω) as the final component of the total internal resistance of the cell. Thus, the linearized portion of the electrode potentials from polarization curves as a function of the current density were fit to $E = R\,j + E_{e0}$, where j is the current density, the slope R is defined as the specific resistance of the anode (R_{An}), cathode (R_{Cat}), or whole MFC (R_{int}) in units of mΩ m^2, and the y-intercepts was used to calculate the experimental open circuit potentials of the anode ($E_{An,e0}$) or cathode ($E_{Cat,e0}$) [13].

Single cycle polarization tests were conducted on the flow-MFC by varying the external resistance (from 1000, 500, 200, 100, 75, 50, 30, 20, 10, 5, 3 Ω at 20 min intervals) after replacing the solution and recording the voltage in open circuit conditions for 2 h, for a total test duration of ~6 h. The voltage drop (U) across an external resistor was recorded by a computer-based data acquisition system (VMP3, Bio-logic, France). Current density (j) and power density (P) were calculated from the current (i) and normalized by the MFC cross-sectional area (A = 7 cm^2) [33]. All potentials are reported here versus SHE. At the end of the polarization test a fast EIS (from 100 kHz to 500 Hz, 5 mV amplitude, 10 points s^{-1}, ≈25 s $scan^{-1}$) was conducted at the OCP to calculate the solution resistance (R_Ω) [31].

3. Results and discussion

3.1. Anode and cathode electrochemical performance

The carbon felt anode acclimated at +200 mV vs SHE showed stable performance after ten days of inoculation with a maximum current density of 6.7 ± 0.3 A m^{-2} from day 10 to day 14 in the chronoamperometry scans (Fig. 3A). In the LSV, the limiting current density, defined as the maximum current density that can be obtained from an electrode reaction [34], was 7.5 ± 0.8 A m^{-2} (peak current density of 8.9 ± 0.8 A m^{-2}) while the anode resistance was R_{An} = 17.5 ± 0.2 mΩ m^2. This R_{An} was 65% larger than that previously reported for graphite fiber brush anodes (R_{An} = 10.6 ± 0.5 mΩ m^2), likely due to the smaller available surface area of the carbon felt compared to that of the brush electrode.

The electrochemical tests on the cathode were performed in an abiotic reactor, to avoid any interference of an anodic biofilm as the counter electrode [6]. The cathode resistance was similar to that of the anode (R_{Cat} = 22.4 ± 0.3 mΩ m^2), and it was slightly smaller in MEA configuration ($R_{Cat\text{-}MEA}$ = 16.5 ± 0.1 mΩ m^2) (Fig. 3B). The lower resistance could be due to the cathode-AEM pressing of the MEA that has been previously showed to reduce the electrode contact resistance [35].

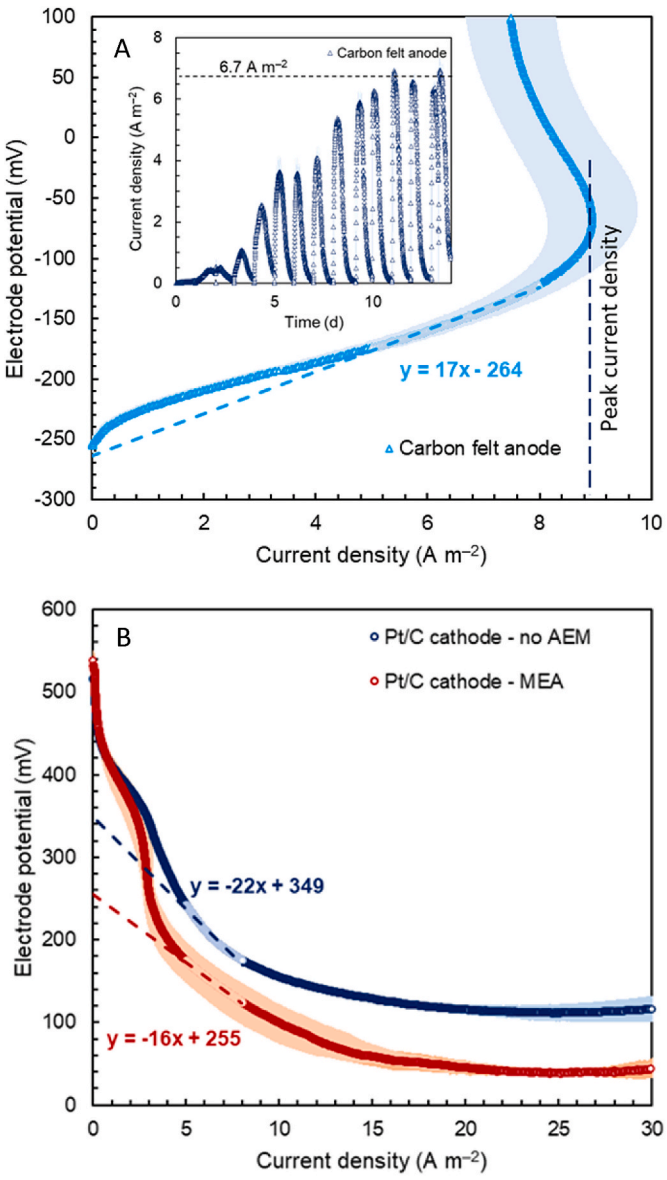

Fig. 3. (A) LSV of the felt anode acclimated at +200 mV in 50 mM PBS for 14 days. Current densities during the acclimation phase are shown in the inset. (B) LSVs of the cathode in the absence of the membrane and cathode in membrane electrode assembly (MEA). The dashed lines represent the linearization of the data in the current density range typical for maximum power generation in MFCs (5–8 A m^{-2}). Electrode potentials that were not corrected for ohmic losses are reported in the Supporting Information.

However, the MEA cold pressing may not have provided enough contact between membrane and electrode, likely reducing the experimental cathode potential ($E_{Cat,e0}$ = 349 ± 2 mV, $E_{Cat,e0\text{-}MEA}$ = 255 ± 1 mV) due to the accumulation of hydroxide ions between the AEM and the catalyst layer (CL) [8].

3.2. Assembled flow MFC performance

The carbon felt anode was transferred into the flow MFC with a new MEA cathode, and stable performance was obtained after two days, producing j = 18.5 ± 0.7 A m^{-2} and P = 4.8 ± 0.3 W m^{-2} (Fig. 4A). Reversing the flow in the anode chamber by recirculating the anolyte from the bottom to the top of the felt slightly increased the performance to j = 19.1 ± 0.7 A m^{-2} and P = 5.1 ± 0.4 W m^{-2}. However, the flow direction was thereafter switched back to the initial flow path.

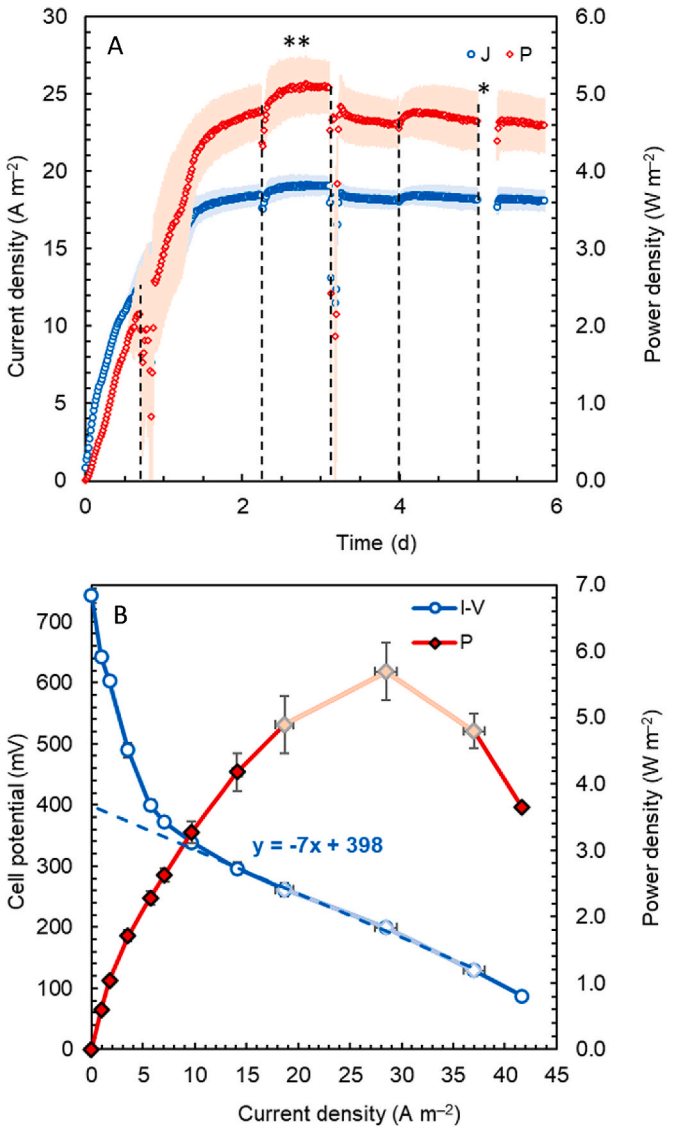

Fig. 4. (A) Power and current density during acclimation in the flow cell with 20 Ω external resistance. The vertical dashed lines indicate when the solution was replaced with a new media. *Polarization test. **The anolyte flow was reversed. (B) Power density and polarization curve of the MFCs. The dashed lines represent the linearization of the data in the maximum power region.

Maximum MFC performance after six days of operation was $j = 18.2 \pm 0.8$ A m^{-2} and $P = 4.7 \pm 0.4$ W m^{-2}, similar to that obtained after two days. The maximum current density generated by the anode felt in LSV was limited by the acidification of the anodic biofilm due to proton generation during acetate oxidation [6]. Assembling the MFC in the AEM-MEA configuration increased the anodic limiting current density by mitigating the anode acidification, resulting in maximum current densities 2× larger than the limiting current density produced by the anode felt in LSVs. The anolyte solution pH did not change over the course of the experiments.

The maximum power density from polarization curves was 5.7 ± 0.4 W m^{-2} (29 ± 1 A m^{-2} with a 10 Ω external resistor). This maximum power density was ~10× larger than that previously reported using a similar MFC configuration and Nafion as a CEM [25], and 54% larger than that obtained using a cloth separator (3.7 W m^{-2}) [14]. This maximum power density is similar to the highest power density ever reported in the literature from a similarly-sized MFC (5.9 ± 0.5 W m^{-2}), although a higher temperature of 40 °C was used in that study compared to 30 °C here, as well as a higher buffer concentration for the electrolyte (70 mM carbonate/phosphate buffer) and additional salts to increase conductivity, compared to 50 mM PBS here [2]. The MFC internal resistance, based on the slope of the polarization curve (Fig. 4B) in the current density range of 19–37 A m^{-2} was only 7.2 ± 0.6 mΩ m^2, with a solution resistance of 1.09 ± 0.02 mΩ m^2 from EIS (Supporting Information). Thus, the anode and cathode resistance accounted for less than 6.1 mΩ m^2 of the total internal resistance, a value much lower than the individual electrode resistances obtained from the LSVs over a current density range of 5–8 A m^{-2} compared to 19–37 A m^{-2} in the polarization curve data (Fig. 3).

3.3. Impact of anolyte and air flow rates on MFC performance

The anolyte flow rate had a large impact on the MFC performance with a 20 Ω external resistance (Fig. 5A). Reducing the anolyte flow rate from 5 mL min^{-1} to 1 mL min^{-1} resulted in erratic performance and average power density over the cycle of 2.9 ± 0.1 W m^{-2}. Increasing the anolyte flow rate up to 15 mL min^{-1} increased the maximum power density to 4.8 ± 0.4 W m^{-2}. This maximum power density did not increase using higher concentrations of acetate in the media (from 2 g L^{-1} to 4 g L^{-1}), thus substate concentration was not limiting the maximum

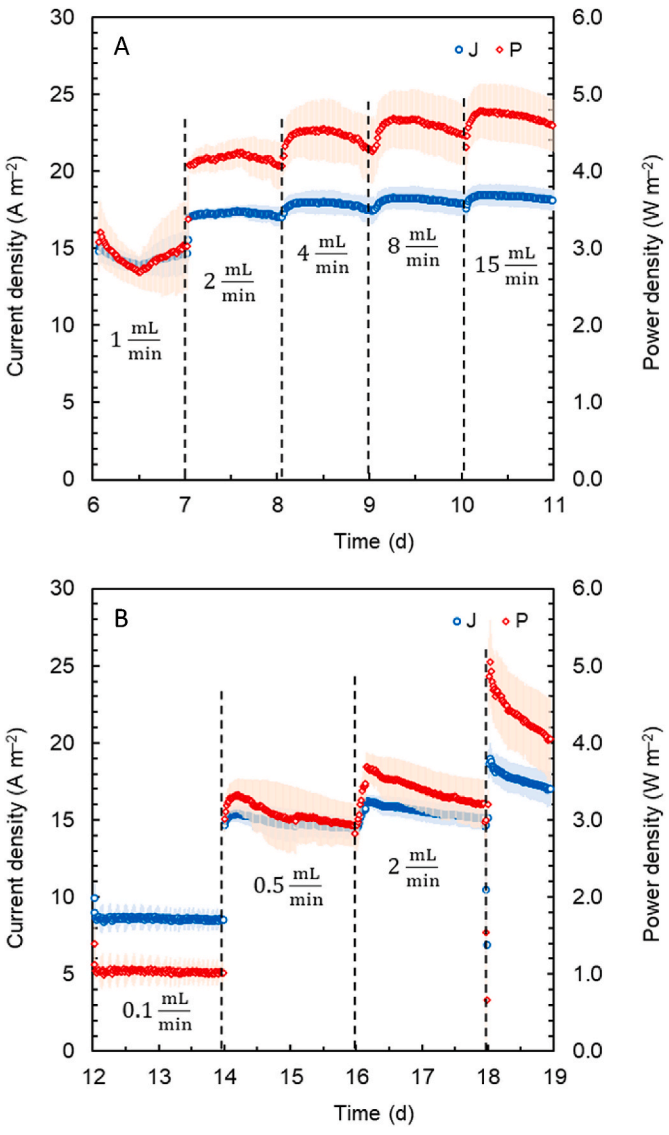

Fig. 5. Impact of (A) anolyte and (B) air flow rate on the flow cell MFC performance.

performance. Coulombic efficiency with 2 g L^{-1} of acetate was stable and >80% for all the flow rate tests with a peak of 98% at 8 mL min^{-1}, but it decreased to 65% with an anolyte flow rate of 15 mL min^{-1} and 4 g L^{-1} acetate.

Reducing the air flow to 0.1 mL min^{-1} from 2 mL min^{-1} (5 mL min^{-1} anolyte) had the largest impact on the performance, reducing the maximum power to only 1.1 ± 0.2 W m^{-2} (Fig. 5B). Likely, oxygen diffusion was limiting the electrochemical reaction at this very low flow rates. Increasing the air flow rate to 0.5 mL min^{-1} increased the performance (3.3 ± 0.2 W m^{-2}). However, following these tests and returning the air flowrate to 2 mL min^{-1}, produced only a maximum power density of 3.7 ± 0.2 W m^{-2}, which was lower than the original maximum power. This reduced power production showed that the original anode activity was not restored, likely due to the prolonged operation at low current density with 0.1 mL min^{-1} air flow. For example, replacing the cathode MEA after 18 days of operation resulted in maximum power density of 5.1 ± 0.5 W m^{-2}, much larger than that initially obtained after assembling the flow-MFC (4.8 ± 0.3 W m^{-2}), but performance was quickly reduced over the cycle length, to 4.1 ± 0.5 W m^{-2}.

3.4. Impact of buffer concentration and solution conductivity on MFC performance

Increasing the buffer concentration improved MFC performance (Fig. 6). Using 100 mM PBS with anolyte flow rate of 5 mL min^{-1} and air flow of 2 mL min^{-1} the maximum power density was 7.1 ± 0.4 W m^{-2} at 45 ± 1 A m^{-2}, 25% larger than that produced with 50 mM PBS (5.7 ± 0.4 W m^{-2}, Fig. 4B). The MFC internal resistance was reduced by 36% to only 4.6 ± 0.2 mΩ m^2 compared to that in 50 mM PBS (7.2 ± 0.6 mΩ m^2). The solution resistance calculated from EIS was only 1.0 ± 0.1 mΩ m^2 (Supporting Information), thus, anode and cathode resistances contributed with only 3.6 mΩ m^2 to the internal resistance. The higher buffer concentration likely reduced the anode diffusion resistance increasing the anodic limiting current density and allowing the production of higher power densities [6].

Feeding the MFC with 50 mM PBS amended with NaCl to match the conductivity of the 100 mM PBS decreased performance, with a maximum power density and internal resistance similar to those obtained with 50 mM PBS (5.6 ± 0.5 W m^{-2} PBS, 5.9 ± 0.4 mΩ m^2, Fig. 6). Thus, the higher performance of the 100 mM PBS with respect to that obtained with 50 mM PBS was due to the higher buffer capacity of the media and not solution conductivity.

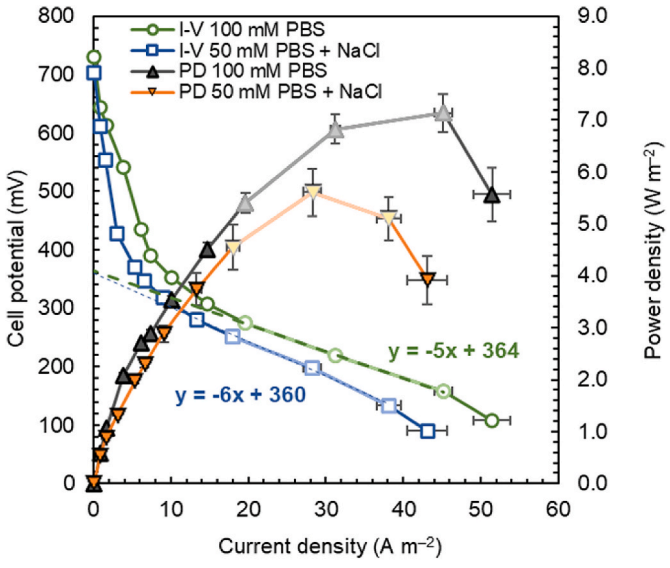

Fig. 6. MFC polarization and power density curves with 100 mM PBS or 50 mM PBS amended with NaCl.

3.5. Insight into the factors impacting the performance of the flow MFC with the AEM configuration

MFCs with an AEM and close electrode spacing in the MEA configuration have never been previously reported in the literature. A comparison of the results obtained here with previous studies using CEMs suggests that the high performance in our study was due to the favorable transport of hydroxide ions from the cathode to balance charge transfer between the electrodes rather than cation transport to the cathode dominated by ions other than protons. It was previously shown that MFC performance was limited by acidification of the anode biofilm, and that adding a buffer to neutralize the solution due to the high rate of protons released from the anode mitigated this phenomenon, increasing the limiting current density [6,7]. However, cloth separators and CEMs do not allow selective ion transport of the products of the electrochemical reactions (H^+ and OH^-) across the separator or membrane. As a result, other ions present at higher concentrations than H^+ and OH^- are transported between the two chambers, leading to large pH imbalances (especially near the electrodes) and decreased MFC performance. An MEA cathode with AEM, and no catholyte, was used here to selectively transport hydroxide ions generated from the ORR away from the cathode, helping to minimize the rise in pH near the cathode catalyst. This enhanced transport from the cathode also helped to more effectively neutralize the pH near the anode as it can become acidified due to H^+ production by the anodic acetate oxidation reaction.

Even with the limited gap between anode and cathode and the AEM selectivity, we observed here that increasing the buffer concentration from 50 mM to 100 mM could further improve performance. Thus, even in our configuration with minimum spacing between the electrodes, a pH difference on the two sides of the AEM must have developed. In addition, it is also likely that not all of the anode biofilm could benefit from hydroxide ion transport through the AEM to create a favorable localized pH. For example, it was previously shown using a more porous brush anode that the microorganisms producing electrical current spanned a distance of at least ~6 mm away from the cathode [36]. Thus, the biofilm on the felt anode used here that were further away from the AEM could still produce protons that might accumulate to concentrations detrimental to power generation due to their distance from the AEM and cathode.

To maximize overall power production in MFCs, the protons produced at the anode and the hydroxide ions produced at the cathode need to be transported towards the other electrode rather than other ions to effectively maintain a neutral pH. Our MFC design used an AEM to selectively transfer hydroxide ions from the cathode to the anode and thus better neutralize protons produced from the anodic biofilm. Even though the higher cost of AEMs compared to non-selective separators could limit their use in MFCs, the better performance of the AEM-based MFCs over time could offset the initial capital investment.

4. Conclusions

The flow cell MFC in MEA configuration with an AEM produced one of the highest power densities of 5.7 ± 0.4 W m^{-2} at 29 ± 1 A m^{-2} in 50 mM PBS. The MFC internal resistance was only 7.2 ± 0.6 mΩ m^2, which was lower than the sum of the anode (R_{An} = 17.5 ± 0.2 mΩ m^2) and cathode resistances ($R_{Cat\text{-}MEA}$ = 16.5 ± 0.1 mΩ m^2) obtained in LSVs. Increasing the anolyte flow rate from 1 mL min^{-1} to 15 mL min^{-1} increased the maximum power density over the cycle from 3.2 ± 0.4 W m^{-2} to 4.8 ± 0.4 W m^{-2}. The air flow rate past the cathode also showed a large impact on the performance, with maximum power densities being 1.1 ± 0.2 W m^{-2} with 1 mL min^{-1} and 3.7 ± 0.2 W m^{-2} with the highest flow rate of 2 mL min^{-1}. The maximum power density with a higher buffer concentration of 100 mM PBS was 7.1 ± 0.4 W m^{-2} at 45 ± 1 A m^{-2}, with an internal resistance of only 4.6 ± 0.2 mΩ m^2, which is to

date the highest power density obtained per cross sectional area in an MFC.

Author contributions

All authors researched data, wrote the article, and reviewed and edited the manuscript before submission.

Declaration of competing interest

The authors declare that they have no known competing financial interests or personal relationships that could have appeared to influence the work reported in this paper.

Acknowledgements

The authors acknowledge funding by the Environmental Security Technology Certification Program via cooperative research agreement W9132T-16-2-0014 through the US Army Engineer Research and Development Center.

Appendix A. Supplementary data

Supplementary data to this article can be found online at https://doi.org/10.1016/j.jpowsour.2020.228633.

References

[1] B.E. Logan, R. Rossi, A. Ragab, P.E. Saikaly, Electroactive microorganisms in bioelectrochemical systems, Nat. Rev. Microbiol. 17 (2019) 307–319, https://doi.org/10.1038/s41579-019-0173-x.
[2] M. Oliot, L. Etcheverry, A. Mosdale, R. Basseguy, M.L. Délia, A. Bergel, Separator electrode assembly (SEA) with 3-dimensional bioanode and removable air-cathode boosts microbial fuel cell performance, J. Power Sources 356 (2017) 389–399, https://doi.org/10.1016/j.jpowsour.2017.03.016.
[3] B.E. Logan, Exoelectrogenic bacteria that power microbial fuel cells, Nat. Rev. Microbiol. 7 (2009) 375–381, https://doi.org/10.1038/nrmicro2113.
[4] S.C. Popat, C.I. Torres, Critical transport rates that limit the performance of microbial electrochemistry technologies, Bioresour. Technol. 215 (2016) 265–273, https://doi.org/10.1016/j.biortech.2016.04.136.
[5] B.E. Rittmann, Ironies in microbial electrochemistry, J. Environ. Eng. 143 (2017), 03117001, https://doi.org/10.1061/(ASCE)EE.1943-7870.0001202.
[6] R. Rossi, D.M. Hall, X. Wang, J.M. Regan, B.E. Logan, Quantifying the factors limiting performance and rates in microbial fuel cells using the electrode potential slope analysis combined with electrical impedance spectroscopy, Electrochim. Acta 348 (2020) 136330, https://doi.org/10.1016/j.electacta.2020.136330.
[7] C.I. Torres, A.K. Marcus, B.E. Rittmann, Proton transport inside the biofilm limits electrical current generation by anode-respiring bacteria, Biotechnol. Bioeng. 100 (2008) 872–881, https://doi.org/10.1002/bit.21821.
[8] S.C. Popat, D. Ki, B.E. Rittmann, C.I. Torres, Importance of OH^- transport from cathodes in microbial fuel cells, ChemSusChem 5 (2012) 1071–1079, https://doi.org/10.1002/cssc.201100777.
[9] R. Rossi, B.E. Logan, Chronoamperometry and linear sweep voltammetry reveals the adverse impact of high carbonate buffer concentrations on anode performance in microbial fuel cells, J. Power Sources (2020) 228715.
[10] W. Yang, B.E. Logan, Immobilization of a metal-nitrogen-carbon catalyst on activated carbon with enhanced cathode performance in microbial fuel cells, ChemSusChem 9 (2016) 2226–2232, https://doi.org/10.1002/cssc.201600573.
[11] Y. Fan, E. Sharbrough, H. Liu, Quantification of the internal resistance distribution of microbial fuel cells, Environ. Sci. Technol. 42 (2008) 8101–8107, https://doi.org/10.1021/es801229j.
[12] R. Rossi, B.E. Logan, Unraveling the contributions of internal resistance components in two-chamber microbial fuel cells using the electrode potential slope analysis, Electrochim. Acta 348 (2020) 136291, https://doi.org/10.1016/j.electacta.2020.136291.
[13] R. Rossi, B.P. Cario, C. Santoro, W. Yang, P.E. Saikaly, B.E. Logan, Evaluation of electrode and solution area-based resistances enables quantitative comparisons of factors impacting microbial fuel cell performance, Environ. Sci. Technol. 53 (2019) 3977–3986, https://doi.org/10.1021/acs.est.8b06004.
[14] Y. Fan, S.K. Han, H. Liu, Improved performance of CEA microbial fuel cells with increased reactor size, Energy Environ. Sci. 5 (2012) 8273–8280, https://doi.org/10.1039/c2ee21964f.
[15] R. Rossi, W. Yang, E. Zikmund, D. Pant, B.E. Logan, In situ biofilm removal from air cathodes in microbial fuel cells treating domestic wastewater, Bioresour. Technol. 265 (2018) 200–206, https://doi.org/10.1016/j.biortech.2018.06.008.
[16] O. Lefebvre, A. Uzabiaga, Y.J. Shen, Z. Tan, Y.P. Cheng, W. Liu, H.Y. Ng, Conception and optimization of a membrane electrode assembly microbial fuel cell (MEA-MFC) for treatment of domestic wastewater, Water Sci. Technol. 64 (2011) 1527–1532, https://doi.org/10.2166/wst.2011.067.
[17] X. Zhang, S. Cheng, X. Huang, B.E. Logan, The use of nylon and glass fiber filter separators with different pore sizes in air-cathode single-chamber microbial fuel cells, Energy Environ. Sci. 3 (2010) 659–664, https://doi.org/10.1039/b927151a.
[18] R.A. Rozendal, H.V.M. Hamelers, C.J.N. Buisman, Effects of membrane cation transport on pH and microbial fuel cell performance, Environ. Sci. Technol. 40 (2006) 5206–5211, https://doi.org/10.1021/es060387r.
[19] B. Kienitz, B. Pivovar, T. Zawodzinski, F.H. Garzon, Cationic contamination effects on polymer electrolyte membrane fuel cell performance, J. Electrochem. Soc. 158 (2011) B1175, https://doi.org/10.1149/1.3610986.
[20] Y. Ahn, B.E. Logan, A multi-electrode continuous flow microbial fuel cell with separator electrode assembly design, Appl. Microbiol. Biotechnol. 93 (2012) 2241–2248, https://doi.org/10.1007/s00253-012-3916-4.
[21] J.L. Stager, X. Zhang, B.E. Logan, Addition of acetate improves stability of power generation using microbial fuel cells treating domestic wastewater, Bioelectrochemistry 118 (2017) 154–160, https://doi.org/10.1016/j.bioelechem.2017.08.002.
[22] S. Kondaveeti, S. Lee, H. Park, B. Min, Specific enrichment of different Geobacter sp . in anode biofilm by varying interspatial distance of electrodes in air-cathode microbial fuel cell (MFC), Electrochim. Acta 331 (2020) 135388, https://doi.org/10.1016/j.electacta.2019.135388.
[23] J. Mi Moon, S. Kondaveeti, T. Ho Lee, Y. Chae Song, B. Min, Minimum interspatial electrode spacing to optimize air-cathode microbial fuel cell operation with a membrane electrode assembly, Bioelectrochemistry 106 (2015) 263–267, https://doi.org/10.1016/j.bioelechem.2015.07.011.
[24] Y. Ahn, B. Logan, Altering anode thickness to improve power production in microbial fuel cells with different electrode distances, Energy Fuels 27 (2013) 271–276, https://doi.org/10.1021/ef3015553.
[25] A.P. Borole, C.Y. Hamilton, T. Vishnivetskaya, D. Leak, C. Andras, Improving power production in acetate-fed microbial fuel cells via enrichment of exoelectrogenic organisms in flow-through systems, Biochem. Eng. J. 48 (2009) 71–80, https://doi.org/10.1016/j.bej.2009.08.008.
[26] Y. Feng, Q. Yang, X. Wang, B.E. Logan, Treatment of carbon fiber brush anodes for improving power generation in air-cathode microbial fuel cells, J. Power Sources 195 (2010) 1841–1844, https://doi.org/10.1016/j.jpowsour.2009.10.030.
[27] E.H. Yu, R. Burkitt, X. Wang, K. Scott, Application of anion exchange ionomer for oxygen reduction catalysts in microbial fuel cells, Electrochem. Commun. 21 (2012) 30–35, https://doi.org/10.1016/j.elecom.2012.05.011.
[28] X. Wang, D. Li, X. Mao, E.H. Yu, K. Scott, E. Zhang, D. Wang, Anion exchange polymer coated graphite granule electrodes for improving the performance of anodes in unbuffered microbial fuel cells, J. Power Sources 330 (2016) 211–218, https://doi.org/10.1016/j.jpowsour.2016.09.019.
[29] S. Cheng, D. Xing, D.F. Call, B.E. Logan, Direct biological conversion of electrical current into methane by electromethanogenesis, Environ. Sci. Technol. 43 (2009) 3953–3958, https://doi.org/10.1021/es803531g.
[30] B. Korth, F. Harnisch, Spotlight on the energy harvest of electroactive microorganisms: the impact of the applied anode potential, Front. Microbiol. 10 (2019) 1–9, https://doi.org/10.3389/fmicb.2019.01352.
[31] B.E. Logan, E. Zikmund, W. Yang, R. Rossi, K.-Y. Kim, P.E. Saikaly, F. Zhang, Impact of ohmic resistance on measured electrode potentials and maximum power production in microbial fuel cells, Environ. Sci. Technol. 52 (2018) 8977–8985, https://doi.org/10.1021/acs.est.8b02055.
[32] F. Zhang, J. Liu, I. Ivanov, M.C. Hatzell, W. Yang, Y. Ahn, B.E. Logan, Reference and counter electrode positions affect electrochemical characterization of bioanodes in different bioelectrochemical systems, Biotechnol. Bioeng. 111 (2014) 1931–1939, https://doi.org/10.1002/bit.25253.
[33] L. Lu, J. Gu, Z.J. Ren, Comment on "Unbiased solar H_2 production with current density up to 23 mA cm-2 by Swiss-cheese black Si coupled with wastewater bioanode,", Energy Environ. Sci. 12 (2019) 3412–3414, https://doi.org/10.1039/c9ee02592h.
[34] F. Yin, P. Hu, C. Song, S. Wang, H. Liu, Unveiling the role of gas permeability in air cathodes and performance enhancement by waterproof membrane fabricating method, J. Power Sources 449 (2020) 227570, https://doi.org/10.1016/j.jpowsour.2019.227570.
[35] S. Ahn, B.J. Tatarchuk, Air electrode: identification of intraelectrode rate phenomena via AC impedance, J. Electrochem. Soc. 142 (2006) 4169, https://doi.org/10.1149/1.2048480.
[36] A.J. Hutchinson, J.C. Tokash, B.E. Logan, Analysis of carbon fiber brush loading in anodes on startup and performance of microbial fuel cells, J. Power Sources 196 (2011) 9213–9219, https://doi.org/10.1016/j.jpowsour.2011.07.040.